Investigation of Shorting Vias for Suppressing the Open Stopband in an SIW Periodic Leaky-Wave Structure

Wenlong Zhou, Juhua Liu, *Member, IEEE,* and Yunliang Long, *Senior Member, IEEE*

***Abstract*— Shorting vias loading in a substrate integrated waveguide (SIW) periodic leaky-wave structure is investigated for suppressing the open stopband. The SIW periodic leaky-wave structure with transverse slots can have the beam scanned in the backward and in the forward directions, but suffers from a large open stopband in which the reflection coefficient is increased and the gain drops drastically. A set of shorting vias are adopted to load the structure in each unit cell for suppressing the open stopband. The working principle of the technique is explained, with approximate equivalent circuits. When the slot and the shorting vias are spaced by a quarter guided wavelength, the series inductance in the slot can be canceled out by the shunt inductance in the shorting vias, and therefore, the open stopband can be suppressed. An antenna based on the via-loaded periodic structure is designed for validation. Simulation and measured results validate that the open stopband is successfully suppressed with the loading of shorting vias.**

***Index Terms*— Open stopband, periodic leaky-wave structure, shorting vias, substrate integrated waveguide (SIW).**

I. Introduction

THE substrate integrated waveguide (SIW) is a recently developed waveguide structure that has a similar propagation property of the conventional rectangular waveguide [1]–[4]. Compared with the conventional rectangular waveguide, the SIW has extra advantages of low profile, lightweight, and easy fabrication. In this century, the SIW has received extensive research and is employed to design various devices, e.g., SIW filters and SIW antennas [5]–[24].

The leaky-wave antenna (LWA) is an attractive traveling-wave antenna, since it has a simple structure and can provide a beam scanned with frequency. A myriad of LWAs have been reported based on various technologies, e.g., rectangular waveguide [25]–[28], microstrip [29]–[32], and SIW [5]–[24]. The SIW LWAs can be distinguished into four categories: uniform [5], [6], quasi-uniform [7]–[10], periodic [11]–[14], and composite right/left handed (CRLH) [15]–[24].

Manuscript received October 1, 2017; revised January 14, 2018; accepted March 16, 2018. Date of publication April 9, 2018; date of current version June 4, 2018. This work was supported in part by the Natural Science Foundation of China under Grant 61771497, Grant 61401522, Grant 41376041, and Grant 61172026 and in part by the NSF of Guangdong Province under Grant 2015A030312010. *(Corresponding author: Juhua Liu.)*

The authors are with the Department of Electronics and Communication Engineering, Sun Yat-sen University, Guangzhou 510006, China (e-mail: liujh33@mail.sysu.edu.cn).

Color versions of one or more of the figures in this paper are available online at http://ieeexplore.ieee.org.

Digital Object Identifier 10.1109/TMTT.2018.2818140

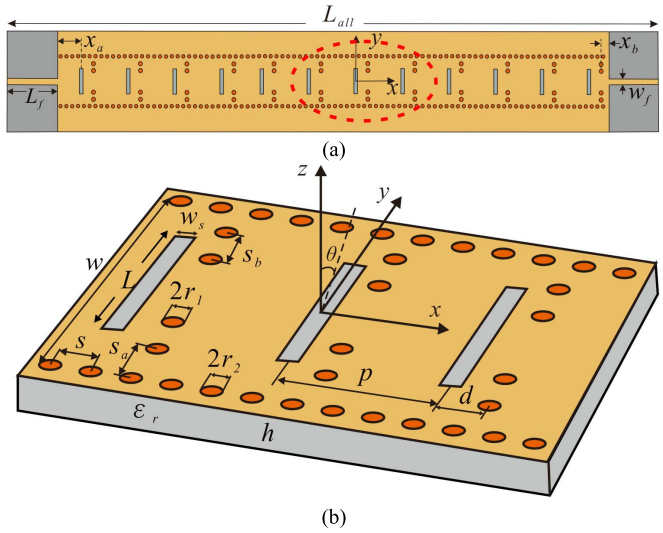

Fig. 1. Geometry of the proposed SIW periodic leaky-wave structure. (a) Overall of the proposed antenna. (b) 3-D geometry of three cells of the periodic leaky-wave structure. The parameters are given in Table I.

The SIW uniform LWA [5], [6] is uniform along the length of the guiding structure, whereas the SIW quasi-uniform LWA [7]–[10] has a periodic structure, in which the periodic is rather small compared to that of the wavelength. In these two types of LWAs, the radiation occurs from the fundamental space harmonic that is a fast wave. The radiation angle θ_0 (measured from the normal direction, i.e., the z-axis in Fig. 1) is determined by the normalized phase constant β/k_0 of the fundamental space harmonic with $\sin\theta_0 = \beta/k_0$. Since the phase constant β is positive, these two kinds of antennas can only have the main beam scanned in the forward quadrant space.

Different from uniform or quasi-uniform structure, the SIW periodic LWA [11]–[14] owns a slow wave fundamental space harmonic, and has a period that is about a guided wavelength in the waveguide (at broadside frequency). The radiation in this type of antenna is contributed by the $n = -1$ space harmonic and the radiation angle is determined by

$$\sin\theta_0 = \beta_{-1}/k_0 \tag{1}$$

where β_{-1} is the phase constant of the $n = -1$ space harmonic calculated by

$$\beta_n = \beta + 2n\pi/p \tag{2}$$

with p the period of the structure. Due to that the phase constant of the $n = -1$ space harmonic can vary from negative to positive, the periodic LWA can have the main beam scanned in the backward and in the forward quadrant spaces. Note that in [8] and [9], an SIW LWA with periodic transverse slots [8] and an SIW LWA with periodic H slots [9] were proposed. Although these two SIW LWAs [8], [9] look quite similar to the SIW LWA investigated in this paper, they belong to the quasi-uniform LWA that can only have the beam scanned in the forward quadrant.

Recently, a number of SIW LWAs based on CRLH metamaterial have been proposed [15]–[24]. Though the structure of this type of LWAs is quasi-uniform and the radiation occurs from the fundamental space harmonic, the main beam can be scanned in the backward and the forward quadrant spaces, owing to the "right-/left-handed" property in the metamaterial.

Although the SIW periodic LWA and the SIW CRLH LWA can have the main beam scanned in the backward and the forward directions, they usually suffer from an open stopband when the main beam is scanned to the broadside. In the open stopband, the reflection coefficient is increased and the gain drops drastically.

Various methods have been proposed for the suppression of the open stopband. In CRLH LWAs [16]–[24], the open stopband can be eliminated based on a "balanced-condition" method.

For periodic LWAs, several methods have been proposed for suppressing the open stopband. In a periodic structure, the unit cell that contains a pair of two identical elements spaced by a quarter of the period can mitigate but cannot completely suppress the open stopband [27]–[30]. A quarter-wave transformer or a matching stub can be used for the complete suppression of the open stopband in a printed periodic LWA [31], [32]. In [33], a printed periodic LWA with the open-stopband suppressed by matching the input impedance of the unit cell to the characteristic impedance of the transmission line was proposed. However, these methods were proposed for a printed periodic structure, and are not so suitable for a rectangular waveguide or an SIW periodic LWA. In [35]–[38], the broadside radiation behavior of a periodic structure was more generally studied from the view of the symmetry or asymmetry in the structure with respect to the longitudinal, or the transverse direction. In [14], an SIW periodic LWA supporting continuous beam scanning from backward to forward was proposed. By introducing additional longitudinal slots as parallel components for unit-cell impedance matching, the SIW periodic LWA can have the open-stopband successfully suppressed. However, the radiation for the antenna in [14] is actually dominated by the longitudinal slots. Since the radiation of each longitudinal slot vanishes at endfires, the scanning range for the antenna in [14] is not very large.

In this paper, we investigate shorting vias for suppressing the open stopband in an SIW periodic leaky-wave structure with transverse slots. In this SIW periodic leaky-wave structure, the leakage is from the slots and through the $n = -1$ space harmonic. The suppression of the open stopband is achieved by loading the structure with a set of shorting vias in each unit cell. The working principle of the technique is investigated, with approximate equivalent circuits. With the circuit analysis, it is found that the slot works dominantly as a series impedance and the shorting vias work dominantly as a shunt admittance. When the slot and the shorting vias are spaced by a quarter guided wavelength, the series inductance in the slot can be canceled out by the shunt inductance in the shorting vias, and therefore the open stopband can be suppressed. An antenna based on the periodic leaky-wave structure is designed for validation. A prototype is fabricated and measured. Simulation and measured results show that the reflection coefficient is greatly lowered and the gain becomes stable, when the open stopband is suppressed with vias loading. With the suppression of the open stopband, the main beam can be scanned seamlessly through broadside, with a wide range from the backward to the forward direction.

TABLE I

PARAMETERS FOR THE PROPOSED SIW PERIODIC LWA AND THE UNIT CELL IN THE EQUIVALENT RECTANGULAR WAVEGUIDE

Symbol	SIW	Rectangular Waveguide		
	Fig. 1	Fig. 2(a)	Fig. 2(b)	Fig. 2(c)
w (mm)	7.93	–	–	–
a (mm)	–	7.4686	7.4686	7.4686
p (mm)	7.5	7.5	7.5	7.5
d (mm)	1.95	–	–	1.9345
L (mm)	4	4	4	4
w_s (mm)	0.5	0.5	0.5	0.5
r_1 (mm)	0.35	–	0.35	0.35
r_2 (mm)	0.3	–	–	–
s (mm)	0.9375	–	–	–
s_a (mm)	1.14	–	1.054	1.054
s_b (mm)	1.11	–	1.015	1.015
x_a (mm)	3.7	–	–	–
x_b (mm)	1.65	–	–	–
x_1 (mm)	–	–	–	1.9
x_2 (mm)	–	–	–	3.6655
$\tan\delta$	0.0023	0	0	0
σ (s/m)	5.8×10^7	∞	∞	∞
W_f (mm)	0.93			
L_f (mm)	8			
L_{all} (mm)	225.8			
h (mm)	1			
ε_r	10.2			

II. APPROXIMATE CIRCUITS FOR THE UNIT CELL OF THE EQUIVALENT RECTANGULAR WAVEGUIDE

In order to suppress the open stopband, we introduce a set of shorting vias for each unit cell of the SIW periodic structure. The geometry of the SIW periodic structure is shown Fig. 1. To simplify the analysis and simulation, we adopt an equivalent rectangular waveguide for the SIW, and assume that the materials (substrate and conductors) are lossless. The equivalent rectangular waveguide has an effective width a [3]. In this section and in Sections III-A and III-B, the simulation results are obtained from simulating a unit cell of the equivalent rectangular waveguide periodic structure. Nevertheless, the dispersion curves from the unit cell are very close to those of the SIW periodic structure with a large number of cells, as will be discussed in Section III-C. The parameters for the SIW and the equivalent rectangular waveguide structure are given in Table I.

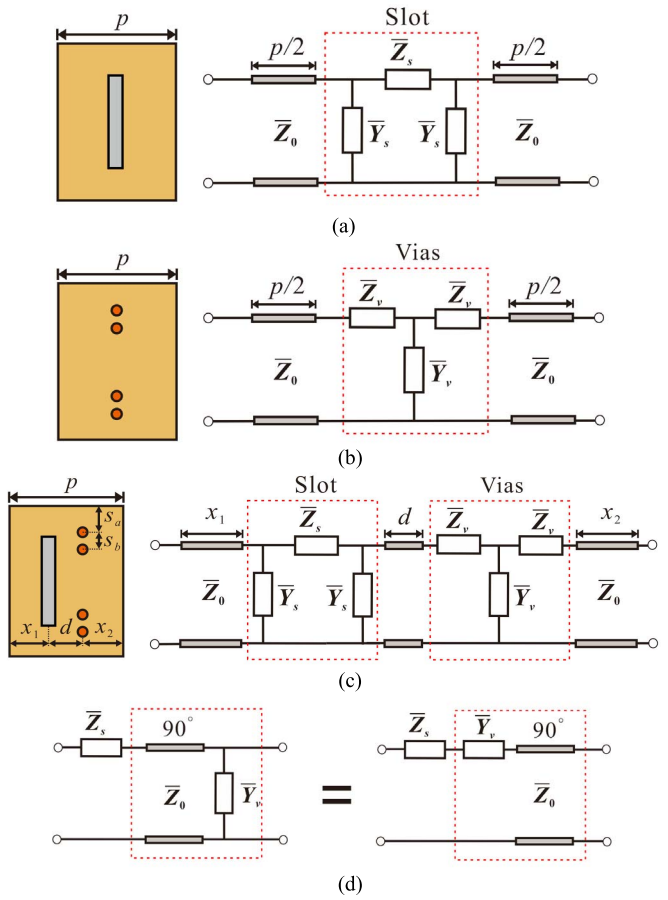

Fig. 2. Approximate circuits for the equivalent rectangular waveguide periodic structures. (a) One slot in the unit cell. (b) Shorting vias in the unit cell. (c) One slot and four vias in the unit cell. (d) Further approximate circuit.

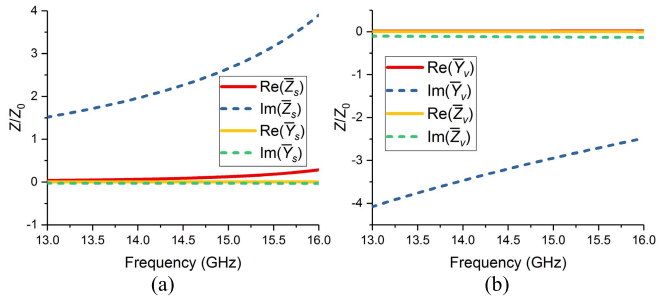

Fig. 3. (a) Normalized series impedance and shunt admittance for the π equivalent circuit of the slot shown in Fig. 2(a). (b) Normalized shunt admittance and series impedance for the T equivalent circuit of the vias shown in Fig. 2(b). The dimensions are given in the third and fourth columns in Table I.

To investigate the working mechanism, we employ approximate circuits to explain the functions of the slot and the shorting vias in the unit cell.

A. Slot in the Unit Cell

When the unit cell contains only one slot but not shorting vias, the slot can be considered as a π equivalent circuit, as shown in the dashed box in Fig. 2(a). In Fig. 2(a),

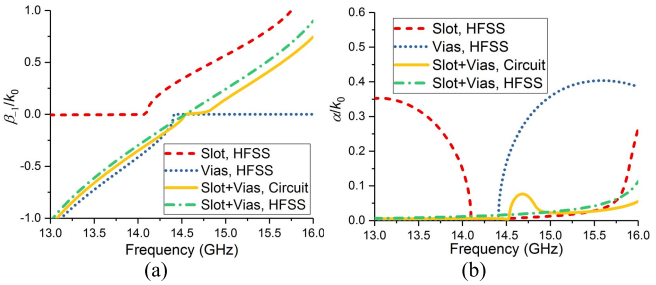

Fig. 4. Normalized (a) phase and (b) attenuation constants for periodic structures with the unit cells shown in Fig. 2. The dimensions are given in Table I.

the equivalent transmission line represents the equivalent rectangular waveguide of the SIW. Note that, all the elements here are normalized by the characteristic impedance Z_0 of the equivalent rectangular waveguide.

We simulate a unit cell of the rectangular waveguide with one slot using HFSS and extract the S-parameters. With the circuit shown in Fig. 2(a), the normalized series impedance $\overline{Z}_s$ and shunt admittance $\overline{Y}_s$ of the slot can be calculated by

$$\overline{Z}_s = \frac{(e^{-j\theta} + S_{11})^2 - S_{21}^2}{2S_{21}e^{-j\theta}} \tag{3}$$

and

$$\overline{Y}_s = \frac{e^{-j\theta} - S_{11} - S_{21}}{e^{-j\theta} + S_{11} + S_{21}} \tag{4}$$

where

$$\theta = \beta_{\text{non}} p \tag{5}$$

and β_{non} represents the phase constant in the unloaded waveguide.

Calculated results for $\overline{Y}_s$ and $\overline{Z}_s$ are shown in Fig. 3(a). It is seen from Fig. 3(a) that the series impedance has a small positive real part due to the leakage effect of the slot. It is also seen that the imaginary part of the impedance is positive, meaning that the slot has an inductive property. The normalized shunt admittance of the slot is purely imaginary and is much smaller than that of the normalized series impedance. Therefore, it is implied that the slot works dominantly as a series inductive element. Due to the slot, the electric current must go around the slot and then the current path is increased, which results in an increase in the series inductance in the transmission line. That is why the slot exhibits a series inductive property.

The wavenumber for a periodic structure can be calculated from the S-parameters of the unit cell by

$$\cos(k_x p) = \frac{1 - S_{11}S_{22} + S_{12}S_{21}}{2S_{21}}. \tag{6}$$

The normalized phase and attenuation constants of the rectangular waveguide periodic structure with slots are shown with dashed lines in Fig. 4. It is seen from Fig. 4 that the periodic structure has a large open stopband.

B. Shorting Vias in the Unit Cell

When the unit cell contains only shorting vias, an approximate circuit shown in Fig. 2(b) can be employed, in which the shorting vias are considered as a T equivalent circuit. With the

circuit shown in Fig. 2(b), the normalized shunt admittance $\overline{Y}_v$ and series impedance $\overline{Z}_v$ can be calculated by

$$\overline{Y}_v = \frac{(e^{-j\theta} - S_{11})^2 - S_{21}^2}{2S_{21}e^{-j\theta}} \tag{7}$$

and

$$\overline{Z}_v = \frac{e^{-j\theta} + S_{11} - S_{21}}{e^{-j\theta} - S_{11} + S_{21}}. \tag{8}$$

Calculated results for $\overline{Y}_v$ and $\overline{Z}_v$ are shown in Fig. 3(b). It is seen from Fig. 3(b) that the shunt admittance and series impedance have almost zero real part, meaning no leakage from the shorting vias. It is also seen that the imaginary part of the admittance is negative, meaning that the vias have an inductive property. The normalized series impedance of the vias is much smaller than that of the normalized shunt admittance. Therefore, it is implied that the vias work dominantly as a shunt inductive element.

The wavenumber of the rectangular waveguide periodic structure with shorting vias can be calculated from the S-parameters of the unit cell by (6). The results are shown with the dotted lines in Fig. 4. Fig. 4 shows that the periodic structure with shorting vias also exhibits a large open stopband.

C. Slot and Shorting Vias in the Unit Cell

When the unit cell contains one slot and shorting vias, an approximate circuit shown in Fig. 2(c) can be employed for the unit cell. The *ABCD* matrix for the network of the unit cell can be calculated by

$$\begin{aligned}\begin{bmatrix} A & B/Z_0 \\ CZ_0 & D \end{bmatrix} &= \begin{bmatrix} \cos\theta_1 & j\sin\theta_1 \\ j\sin\theta_1 & \cos\theta_1 \end{bmatrix} \\ &\times \begin{bmatrix} 1+\overline{Y}_s\overline{Z}_s & \overline{Z}_s \\ 2\overline{Y}_s + \overline{Z}_s\overline{Y}_s^2 & 1+\overline{Y}_s\overline{Z}_s \end{bmatrix} \begin{bmatrix} \cos\theta_s & j\sin\theta_s \\ j\sin\theta_s & \cos\theta_s \end{bmatrix} \\ &\times \begin{bmatrix} 1+\overline{Y}_v\overline{Z}_v & 2\overline{Z}_v + \overline{Y}_v\overline{Z}_v^2 \\ \overline{Y}_v & 1+\overline{Y}_v\overline{Z}_v \end{bmatrix} \begin{bmatrix} \cos\theta_2 & j\sin\theta_2 \\ j\sin\theta_2 & \cos\theta_2 \end{bmatrix} \end{aligned} \tag{9}$$

where

$$\theta_1 = \beta_{\text{non}} x_1 \quad \theta_s = \beta_{\text{non}} d \quad \theta_2 = \beta_{\text{non}} x_2 \tag{10}$$

and

$$x_1 + d + x_2 = p. \tag{11}$$

With the calculated *ABCD* matrix, the wavenumber of the related periodic structure can be calculated by [43]

$$\cos(k_x p) = (A + D)/2. \tag{12}$$

With the results for $\overline{Y}_s$ and $\overline{Z}_s$ of the slot and $\overline{Y}_v$ and $\overline{Z}_v$ of the vias calculated in Sections II-A and II-B, the wavenumber can be calculated with (9)–(12). The calculated phase and attenuation constants are shown with the dashed-dotted lines in Fig. 4. It is seen that the open stopband is significantly suppressed compared with the structure with only slot or vias. The wavenumber can also be calculated by (6), from the S-parameters extracted directly from HFSS. The result for the wavenumber from HFSS shows that the periodic structure has the open stopband completely suppressed. Since the approximate circuit in Fig. 2(c) neglects the coupling effect between the slot and the shorting vias, a small discrepancy is observed between the result from the approximate circuit and that from HFSS. Nevertheless, the two results are close, especially, for the normalized phase constant.

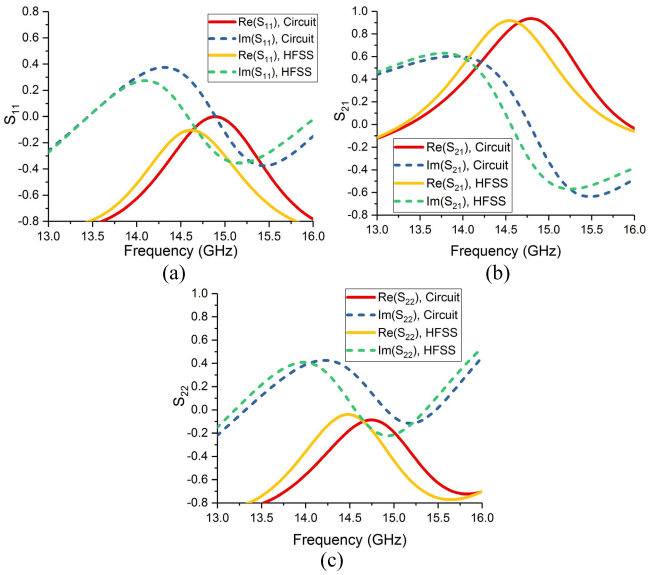

Fig. 5. (a) S_{11}, (b) S_{21}, and (c) S_{22} parameters for the unit cell shown in Fig. 2(c). The dimensions are given in the fifth column in Table I.

With the calculated results for $\overline{Y}_s$, $\overline{Z}_s$, $\overline{Y}_v$, and $\overline{Z}_v$ from Sections II-A and II-B, the *ABCD* matrix can be calculated by (9). Then, the S-parameter can be obtained from the *ABCD* matrix by [43]. The calculated S-parameters for the approximate circuit are shown in Fig. 5. It is seen that the S-parameters calculated with the approximate circuit are very close to those extracted directly from the simulation using HFSS.

D. Further Approximation

Since the slot works dominantly as a series element and the shorting vias work dominantly as a shunt element, we can use a more approximate circuit shown in the left circuit in Fig. 2(d) to represent the slot, the shorting vias, and the waveguide between them. Suppose that the distance between the two elements is a quarter guided wavelength, namely, $\beta_{\text{non}} d = 90°$. Then, the *ABCD* matrix (in normalized form) for the subnetwork in dashed box in the left circuit in Fig. 2(d) can be represented as

$$\begin{bmatrix} A & B/Z_0 \\ CZ_0 & D \end{bmatrix} = \begin{bmatrix} 0 & j \\ j & 0 \end{bmatrix} \begin{bmatrix} 1 & 0 \\ \overline{Y}_v & 1 \end{bmatrix} = \begin{bmatrix} j\overline{Y}_v & j \\ j & 0 \end{bmatrix}. \tag{13}$$

Similarly, the *ABCD* matrix for the subnetwork in dashed box in the right circuit in Fig. 2(d) can be calculated by

$$\begin{bmatrix} A & B/Z_0 \\ CZ_0 & D \end{bmatrix} = \begin{bmatrix} 1 & \overline{Y}_v \\ 0 & 1 \end{bmatrix} \begin{bmatrix} 0 & j \\ j & 0 \end{bmatrix} = \begin{bmatrix} j\overline{Y}_v & j \\ j & 0 \end{bmatrix}. \tag{14}$$

With (13) and (14), the two subnetworks have the same *ABCD* matrixes. Therefore, the left and the right circuits in Fig. 2(d) have the same performance. With Fig. 2(d), we can see that when a (shunt) element is moved backward by a quarter guided wavelength, the shunt element is changed to a series element with the same normalized value.

Therefore, the left circuit [in Fig. 2(d)] that includes a series element and a shunt element is equivalently changed to the right circuit that includes two series elements. The total impedance of the series elements becomes $\overline{Z}_s + \overline{Y}_v$. When the imaginary part of $\overline{Z}_s$ is opposite to the imaginary part of $\overline{Y}_v$ (it is also assumed that the real parts of the two parameters are very small or zero), the sum of $\overline{Z}_s + \overline{Y}_v$ becomes very small or zero, and therefore the open stopband can be suppressed.

From Fig. 3, it is seen that the imaginary part of $\overline{Z}_s$ is almost opposite to the imaginary part of $\overline{Y}_v$ (at broadside frequency), and the real part of $\overline{Z}_s$ is very small. (The real part of $\overline{Y}_v$ is 0.) Besides, the distance d between the slot and the shorting vias is about a quarter guided wavelength, namely,

$$d \approx \lambda_g/4 = \pi/(2\beta_{\text{non}}). \tag{15}$$

Therefore, the proposed structure of slot and shorting vias can have the open-stopband suppressed.

At broadside frequency, we have $\beta_{-1} = 0$ with (2). Then, we have $2\pi/\beta = p$. When the sum of $\overline{Z}_s + \overline{Y}_v$ is very small, the propagation phase constant β in the periodic structure approximately equals to the phase constant β_{non} in the unperturbed waveguide. With (15), we have

$$d \approx p/4. \tag{16}$$

Therefore, in the design for the slot and shorting vias, the distance d should be approximately a quarter of the period.

III. Antenna Design

A. Parameter Study of the Shorting Vias

In this section, the design of shorting vias for suppressing the open stopband is studied with simulation using HFSS. There are several parameters that have effects on the open-stopband suppression, including the radius of the via (r_1), the distance between the slot and the shorting via (d), the distance of the via from the edge of waveguide (s_a), the distance between the vias (s_b), and the number of the shorting vias.

Fig. 6(a) shows the normalized attenuation constant for the unit cell with different distances d between the slot and the shorting vias. It is seen that the attenuation constant is sensitive to the distance. With the circuit analysis in Section II-D, it is implied that distance d plays an important role and should be around a quarter of the period ($p/4$) for the open-stopband suppression. With the simulation results shown in Fig. 6(a), it is seen that the optimized value of $d = 1.935$ mm is very close to $p/4 = 1.875$ mm.

Fig. 6(b) shows the normalized attenuation constant for shorting vias with different radii. With the increase of the radius, the attenuation constant is effected due to that the increase in the radius results in an increase in the shunt inductance.

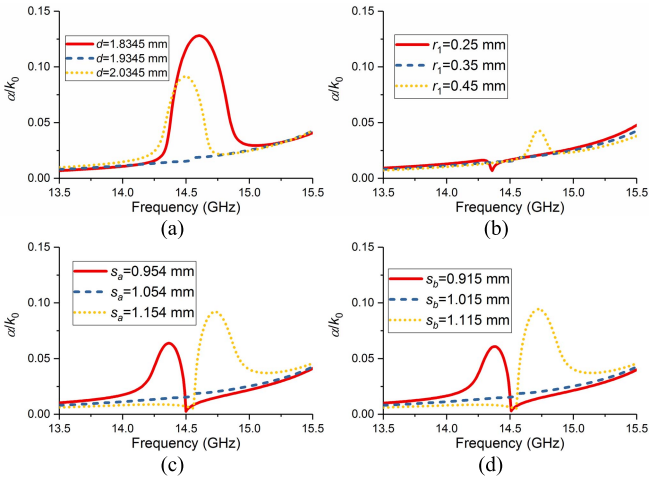

Fig. 6. Results simulated from the unit cell by HFSS. (a) Attenuation constants versus d. (b) Attenuation constants versus r_1. (c) Attenuation constants versus s_a. (d) Attenuation constants versus s_b.

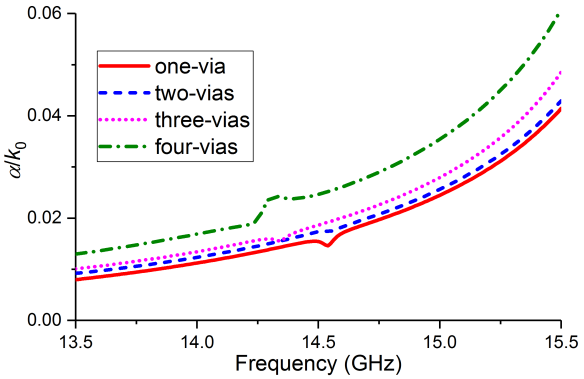

Fig. 7. Normalized attenuation constants simulated from the unit cell with different numbers of shorting vias at each side. The dimensions are given in Table II.

Fig. 6(c) shows the normalized attenuation constant with different distances (s_a) of the via from the edge of waveguide, with the geometry shown in Fig. 2(c). Fig. 6(d) shows the normalized attenuation constant with different distances between the vias (s_b). It is seen from Fig. 6(c) and (d) that the two parameters (s_a and s_b) have significant effects on the open stopband due to that the two parameters play major roles on the equivalent shunt admittance of the shorting vias. The analysis in Section II-D reveals that only the imaginary part of the normalized shunt admittance of the shorting vias can cancel out the imaginary part of the normalized series impedance of the slot, the open stopband can be well suppressed.

Fig. 7 shows the normalized attenuation constant for the unit cell with different numbers of shorting vias at each side (e.g., the side for $y > 0$ in Fig. 1). Note that these results are with the optimized parameters given in Table II for the open-stopband suppression. It is seen from Fig. 7 that the open stopband can be suppressed, with different numbers of shorting vias. However, when a larger number of shorting vias are adopted, the radius of the shorting vias should be smaller, since the shunt inductance of each shorting via with smaller radius is

TABLE II
PARAMETERS FOR THE UNIT CELL IN FIG. 7

Symbol	amounts of the shorting vias per side			
	One	Two	Three	Four
d (mm)	1.94	1.935	1.94	1.94
r_1 (mm)	0.4	0.35	0.2	0.15
s_a (mm)	2	1.015	1.01	0.82
s_b (mm)	-	1.054	0.62	0.5

*Other parameters are the same as those in the fifth column in Table I.

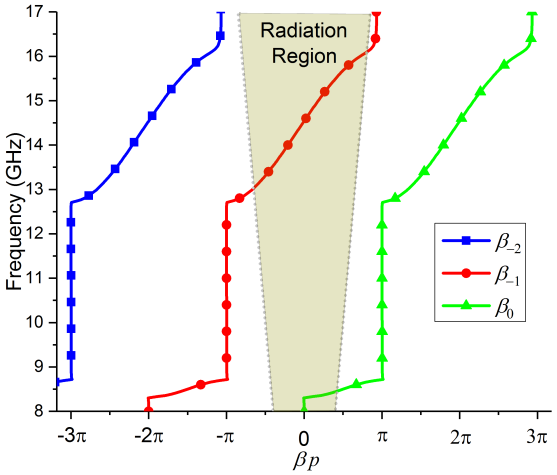

Fig. 8. Brillouin diagram for the optimized unit cell shown in Fig. 2(c).

smaller, whereas the total shunt admittance of the shorting vias needs to remain the same. Since it becomes difficult and sensitive for fabrication if a large number of shorting vias with small radius are used, we choose two vias with medium radius for each side in the unit cell.

B. Single-Beam Radiation

In the periodic LWA, the radiation is contributed by $n = -1$ space harmonic. In order to have only one beam scanning, radiation from other space harmonics (e.g., $n = 0$ and $n = -2$) should be avoided.

In this equivalent rectangular waveguide structure, the fundamental space harmonic has a fast-wave region that is nearby the cutoff frequency of the waveguide. In the antenna design, this fast-wave region in the fundamental space harmonic should be avoided.

As frequency increases, the $n = -2$ space harmonic may enter into fast-wave region. In order to avoid the radiation from the $n = -2$ space harmonic, a substrate with higher permittivity can be used [26].

Fig. 8 shows the Brillouin diagram for the equivalent rectangular waveguide periodic structure. It is seen that in the operation band from 13.02 to 16.1 GHz, only the $n = -1$ space harmonic is in the fast-wave region (shaded region in Fig. 8), and other space harmonics (e.g., $n = 0$ and $n = -2$) are not in the fast-wave region. Although a fast-wave region (from 8.3 to 8.455 GHz) in the fundamental space harmonic occurs nearby the cutoff frequency (8.3 GHz), the region is far from the operation band of the presented periodic antenna.

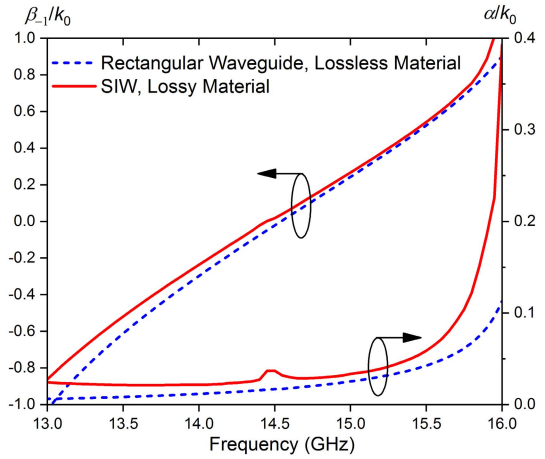

Fig. 9. Normalized phase and attenuation constants for the periodic SIW leaky-wave structures and the equivalent rectangular waveguide structure.

C. Dispersion Curves for the SIW Periodic Leaky-Wave Structure

In the above analyses, we simulate a unit cell of the equivalent rectangular waveguide periodic structure with no material loss. Here, we simulate an SIW periodic structure with 28 cells and extracted the wavenumber from the near fields inside the SIW [8]. In the simulation, the material losses are also be concerned. For the SIW periodic structure, the parameters for the shorting-vias require a further but very slight optimization, based on those for the unit cell in the rectangular waveguide structure. The parameters for the SIW periodic structure is given in the second column in Table I.

Fig. 9 shows the normalized phase and attenuation constants for the SIW periodic structure. The phase and attenuation constants for the equivalent rectangular waveguide are also demonstrated, from simulation of only one unit cell. Fig. 9 shows that the phase and attenuation constants of the SIW periodic structure are very close to those of the equivalent rectangular periodic structure. With the material losses concerned in the SIW structure, the attenuation constant in the SIW structure is higher than that in the equivalent rectangular waveguide of no material loss.

IV. EXPERIMENTS

In order to validate the open-stopband suppression in the periodic structure, an LWA based on the structure is designed. The geometry of the design is shown in Fig. 1. A prototype of the SIW periodic LWA with vias loading is fabricated and measured. The photograph of the fabricated antenna is shown in Fig. 10. The antenna is fabricated on a substrate with a relative permittivity of 10.2, a loss tangent of $\tan\delta = 0.0023$, and a thickness of 1 mm. The antenna is fed by a microstrip line with a characteristic impedance of 50 Ω and is terminated by a 50-Ω load.

Fig. 11 shows the reflection coefficient (S_{11}) and transmission coefficient (S_{21}) for the proposed antenna. It is seen that measured result is close to simulation result, although a small shift of frequency is observed due to fabrication errors.

Fig. 10. Top and bottom views of the fabricated SIW LWA.

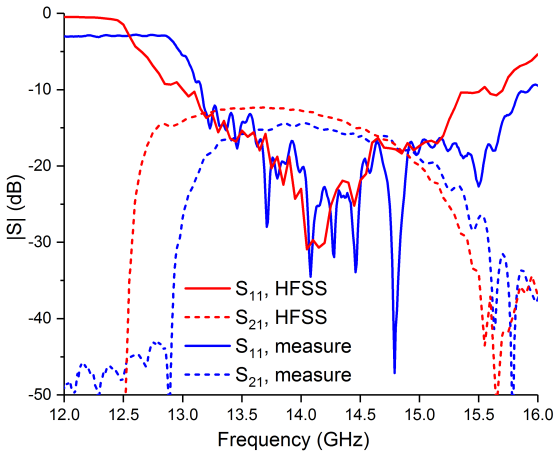

Fig. 11. Reflection and transmission coefficients for the antenna in Fig. 10.

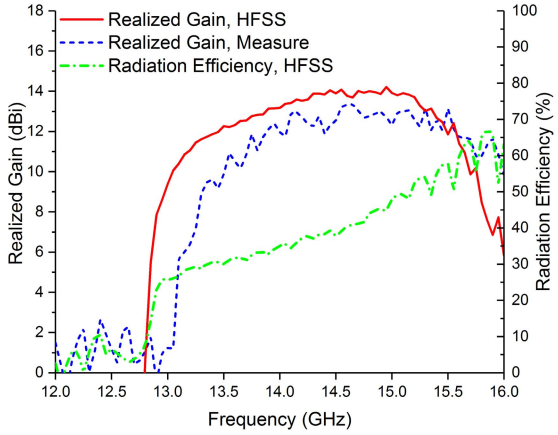

Fig. 12. Realized gain (that accounts for the reflection coefficient) and efficiency for the antenna (shown in Fig. 10).

Around the broadside frequency (around 14.5 GHz), both the simulation and measured results for the reflection coefficient are lower than −15 dB, meaning that a good input impedance match is achieved. No significant drop in the transmission coefficient (in either the simulation or measured result) is observed around the broadside frequency. The transmission coefficient is lower than −10 dB, meaning that less than 10% of the power is left at the end of the antenna.

Fig. 12 shows the measured and simulated realized gain for the proposed antenna. It is seen that the measured gain is a little lower (about 1.5 dB) than the simulation result, probably due to the insertion loss caused by the SMA and measurement errors. In a band from 13.2 to 15.6 GHz, the simulated gain is up to 14.1 dBi, with a variation within 3 dB. The gain remains almost stable around the broadside frequency.

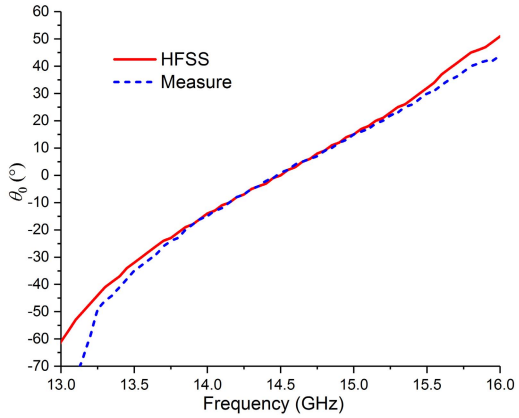

Fig. 13. Radiation angle for the antenna (shown in Fig. 10).

Fig. 12 also shows the radiation efficiency for the proposed antenna. It is observed that the radiation efficiency is about 30%–60% in the operating band. The low radiation is not due to the introduction of the shorting vias. (While not shown here, the radiation efficiency for the SIW periodic LWA without shorting vias loading is only about 30%–60%.) The low radiation efficiency is caused by the material loss in the substrate and the conductors (copper). A substrate of lower tangent loss or a conductor with higher conductivity can be used for the improvement of the efficiency.

Fig. 13 shows the radiation angle [the main beam direction measured from the z-axis, as shown in Fig. 1(b)] against the frequency. It is found that the measured result is almost consistent with the simulation result. The simulation result shows that the main beam can be scanned from −47° to 37°, when the frequency increases from 13.2 to 15.6 GHz (where the variation of the realized gain is within 3 dB). The main beam of the via-loaded antenna can be scanned seamlessly through broadside. Around broadside (around 14.5 GHz), the radiation angle increases almost linearly with the frequency.

Fig. 14 shows the realized gain patterns of the via-loaded antenna working at different frequencies (from 13.6 to 15.4 GHz), in the principle scanning plane (xz plane). It is observed that the measured results are almost consistent with the simulation results except that the measured gain is a little lower. At 14.5 GHz, the main beam is in the broadside direction and does not suffer from a degradation. Around broadside, the beamwidth of the antenna keeps almost stable.

Fig. 15 shows the radiation patterns for the antenna at broadside, in the xz plane and in the yz plane. In the xz plane, it is seen that the antenna has a narrow beam with a beamwidth of 5.5°. In the yz plane, the antenna has a fan beam with a beamwidth of 16.5°.

From Figs. 11–15, it is confirmed that the technique of shorting vias can indeed completely suppress the open-stopband effects. With the loading of shorting vias,

TABLE III
COMPARISON WITH OTHER CONTINUOUSLY SCANNING PLANAR LWAS

Ref.	Antenna Type	ε_r	Total Length (λ_0)	Bandwidth (%)	Single-Beam Scanning Range	Max Realized Gain (dBi)	Applied Structure
[8]	quasi-uniform, SIW	2.25	8.89	16.2%(10.2–12 GHz)	57º (15º ~ 72º)	14	–
[32]	Periodic, microstrip	2.2	11.64	35.1% (8–11.4 GHz)	35º (–25º ~ 10º)	16	printed structure
[33]	Periodic, microstrip	6.15	7.6	36.7% (20–29 GHz)	95º (–50º ~ 45º)	12.2	printed structure
[16]	CRLH, multilayer SIW	2.2	6.25	38.6% (8.25–12.2 GHz)	158º (–78º ~ 80º)	11.5	printed structure
[18]	CRLH, multilayer SIW	2.2	7	44.7% (8.25–13 GHz)	126º (–60º ~ 66º)	12	printed structure
[20]	CRLH, SIW	2.2	5.17	14.6% (24–27.73 GHz)	30º (–17º ~ 13º)	14	printed structure
[21]	CRLH, SIW	2.2	4.2	34.2% (8.5–12 GHz)	130º (–70º ~ 60º)	10.8	printed structure
[22]	CRLH, multilayer SIW	2.2	6	47.6% (8–13 GHz)	147º (–72º ~ 75º)	12.6	printed structure
[14]	Periodic SIW	3.66	5.61	43.5% (9–14 GHz)	75º (–40º ~ 35º)	12	waveguide, SIW
ours	Periodic SIW	10.2	11.12	16.1% (13.2–15.6 GHz)	103º (–61º ~ 42º)	14.1	printed structure, waveguide, SIW

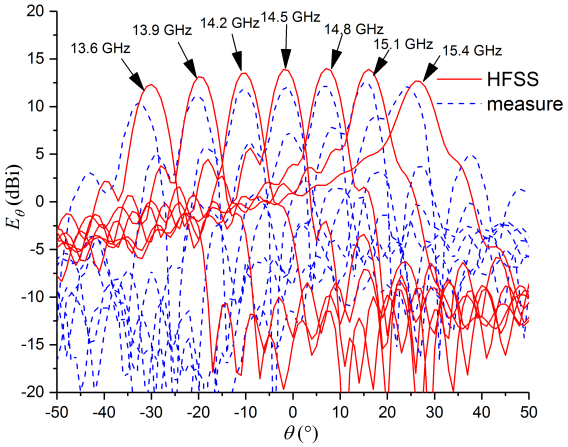

Fig. 14. Realized gain patterns of the co-polarized fields for the antenna (shown in Fig. 10) in the principle plane (*xz* plane).

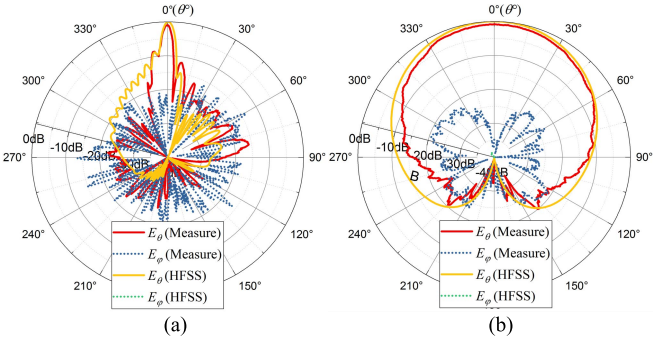

Fig. 15. Normalized radiation patterns for the antenna in Fig. 10. (a) Radiation patterns in the *xz* plane. (b) Radiation patterns in the *yz* plane.

the SIW periodic LWA can have the main beam scanned seamlessly from backward to forward, with a stable gain and no standstill around broadside.

V. COMPARISONS

Table III illuminates the comparison of our proposed technique and those in published papers.

In SIW LWAs, most of the published techniques were reported for the open-stopband suppression for CRLH LWAs [16], [18], [20]–[22]. In these published structures, the open stopband is successfully suppressed with the balance condition. However, the CRLH LWAs, in principle, belong to the quasi-uniform LWA category, in which the period is much smaller than a wavelength in free space. These methods are not suitable for a periodic LWA in which the periodic is about a guided wavelength. For printed periodic LWAs, some methods were proposed, such as quarter-wave transformer, matching stub [32], and unit-cell impedance matching [33]. However, these methods were designed for a microstrip periodic structure and are not so suitable for an SIW or a rectangular waveguide structure. In [14], a method for suppressing the open-stopband in an SIW periodic LWA is proposed, by introducing a longitudinal slot for each unit cell. However, the radiation for the antenna in [14] is dominated by the longitudinal slots. Since the radiation pattern for each longitudinal slot vanishes at endfires, the scanning range is not very large [14].

In this paper, we proposed a method to suppress the open stopband in an SIW periodic LWA by shorting vias. This method is simple and effective for periodic LWA. Compared with the antenna in [14], the radiation is generated by the transverse slots (each of which has an omnidirectional radiation pattern in the principle scanning plane in the upper half-space), so that the scanning range can be enlarged.

VI. CONCLUSION

Shorting vias for suppressing the open stopband in an SIW periodic leaky-wave structure have been presented and investigated. The working principle of the suppression of the open stopband is explained with approximate circuits. With the analyses, it is found that the slot works dominantly as a series impedance and the shorting vias work dominantly as a shunt admittance. When the slot and the shorting vias are spaced by a quarter of the guided wavelength, the series inductance in the slot can be canceled out by the shunt inductance in the shorting vias, and therefore the open stopband can be

suppressed. In order to validate the effects of the technique, an LWA based on the periodic structure is designed, fabricated and measured. Measured results agree with simulation results. The results demonstrate that the open stopband has been completely suppressed with the technique using shorting vias. With the open stopband suppressed, the reflection coefficient is lowered around broadside, and the main beam can be scanned seamlessly through broadside with a stable gain and with a wide range from backward to forward.

Besides the open-stopband suppression of the SIW LWA, the technique investigated in this paper, in which the imaginary part in the normalized impedance of a series element can be canceled out by the imaginary part in the normalized admittance of a shunt element spaced by a quarter period, can be developed for the open-stopband suppression in other periodic leaky-wave structures (e.g., rectangular waveguide and microstrip line), or impedance matching for a circuit.

ACKNOWLEDGMENT

The authors would like to thank the reviewers for their useful suggestions that have helped to improve this paper.

REFERENCES

[1] J. Hirokawa and M. Ando, "Single-layer feed waveguide consisting of posts for plane TEM wave excitation in parallel plates," *IEEE Trans. Antennas Propag.*, vol. 46, no. 5, pp. 625–630, May 1998.

[2] D. Deslandes and K. Wu, "Integrated microstrip and rectangular waveguide in planar form," *IEEE Microw. Wireless Compon. Lett.*, vol. 11, no. 2, pp. 68–70, Feb. 2001.

[3] L. Yan, W. Hong, K. Wu, and T. J. Cui, "Investigations on the propagation characteristics of the substrate integrated waveguide based on the method of lines," *Proc. Inst. Elect. Eng.—Microw., Antennas Propag.*, vol. 152, no. 1, pp. 35–42, Feb. 2005.

[4] F. Xu and K. Wu, "Guided-wave and leakage characteristics of substrate integrated waveguide," *IEEE Trans. Microw. Theory Techn.*, vol. 53, no. 1, pp. 66–73, Jan. 2005.

[5] J. Xu, W. Hong, H. Tang, Z. Kuai, and K. Wu, "Half-mode substrate integrated waveguide (HMSIW) leaky-wave antenna for millimeter-wave applications," *IEEE Antennas Wireless Propag. Lett.*, vol. 7, pp. 85–88, Apr. 2008.

[6] Y. J. Cheng, W. Hong, K. Wu, and Y. Fan, "Millimeter-wave substrate integrated waveguide long slot leaky-wave antennas and two-dimensional multibeam applications," *IEEE Trans. Antennas Propag.*, vol. 59, no. 1, pp. 40–47, Jan. 2011.

[7] D. Deslandes and K. Wu, "Substrate integrated waveguide leaky-wave antenna: Concept and design considerations," in *Proc. Asia–Pacific Microw. Conf.*, Dec. 2005, pp. 346–349.

[8] J. Liu, D. R. Jackson, and Y. Long, "Substrate integrated waveguide (SIW) leaky-wave antenna with transverse slots," *IEEE Trans. Antennas Propag.*, vol. 60, no. 1, pp. 20–29, Jan. 2012.

[9] J. Liu, X. Tang, Y. Li, and Y. Long, "Substrate integrated waveguide leaky-wave antenna with H-shaped slots," *IEEE Trans. Antennas Propag.*, vol. 60, no. 8, pp. 3962–3967, Aug. 2012.

[10] A. J. Martinez-Ros, J. L. Gómez-Tornero, and G. Goussetis, "Holographic pattern synthesis with modulated substrate integrated waveguide line-source leaky-wave antennas," *IEEE Trans. Antennas Propag.*, vol. 61, no. 7, pp. 3466–3474, Jul. 2013.

[11] F. Xu, K. Wu, and X. Zhang, "Periodic leaky-wave antenna for millimeter wave applications based on substrate integrated waveguide," *IEEE Trans. Antennas Propag.*, vol. 58, no. 2, pp. 340–347, Feb. 2010.

[12] Y. Cheng, W. Hong, and K. Wu, "Millimeter-wave half mode substrate integrated waveguide frequency scanning antenna with Quadri-polarization," *IEEE Trans. Antennas Propag.*, vol. 58, no. 6, pp. 1848–1855, Jun. 2010.

[13] R. Henry and M. Okoniewski, "A broadside scanning substrate integrated waveguide periodic phase-reversal leaky-wave antenna," *IEEE Antennas Wireless Propag. Lett.*, vol. 15, pp. 602–605, 2015.

[14] Y. L. Lyu *et al.*, "Leaky-wave antennas based on noncutoff substrate integrated waveguide supporting beam scanning from backward to forward," *IEEE Trans. Antennas Propag.*, vol. 64, no. 6, pp. 2155–2164, Jun. 2016.

[15] C. Caloz and T. Itoh, *Electromagnetic Metamaterials Transmission Line Theory and Microwave Applications*. New York, NY, USA: Wiley, 2005.

[16] Q. Zhang, G. C. Wu, G. M. Wang, J. G. Liang, and X. J. Gao, "Beam scanning antenna with wideband broadside radiation based on multilayered substrate integrated waveguide composite right/left-handed structure," *Frequenz*, vol. 71, nos. 1–2, pp. 29–35, 2017.

[17] R. Agrawal, "Continuous beam scanning in substrate integrated waveguide leaky wave antenna," *Prog. Electromagn. Res.*, vol. 62, pp. 19–28, 2017.

[18] Nasimuddin, Z. N. Chen, and X. Qing, "Substrate integrated metamaterial-based leaky-wave antenna with improved boresight radiation bandwidth," *IEEE Trans. Antennas Propag.*, vol. 61, no. 7, pp. 3451–3457, Jul. 2013.

[19] A. Pourghorban Saghati, M. M. Mirsalehi, and M. H. Neshati, "A HMSIW circularly polarized leaky-wave antenna with backward, broadside, and forward radiation," *IEEE Antennas Wireless Propag. Lett.*, vol. 13, pp. 451–454, 2014.

[20] W. Cao, Z. N. Chen, W. Hong, B. Zhang, and A. Liu, "A beam scanning leaky-wave slot antenna with enhanced scanning angle range and flat gain characteristic using composite phase-shifting transmission line," *IEEE Trans. Antennas Propag.*, vol. 62, no. 11, pp. 5871–5875, Nov. 2014.

[21] Y. D. Dong and T. Itoh, "Composite right/left-handed substrate integrated waveguide and half mode substrate integrated waveguide leaky-wave structures," *IEEE Trans. Antennas Propag.*, vol. 59, no. 3, pp. 767–775, Mar. 2011.

[22] Nasimuddin, Z. N. Chen, and X. Qing, "Tapered composite right/left-handed leaky-wave antenna for wideband broadside radiation," *Microw. Opt. Technol. Lett.*, vol. 57, no. 3, pp. 624–629, 2015.

[23] G. C. Wu, G. M. Wang, J. G. Liang, and X. J. Gao, "Wideband leaky-wave antenna with consistent gain and wide beam scanning angle based on multilayered substrate integrated waveguide composite right/left-handed transmission line," *Int. J. RF Microw. Comput. Eng.*, vol. 26, no. 8, pp. 731–738, 2016.

[24] G. C. Wu, G. M. Wang, X. J. Gao, and J. G. Liang, "Wideband dual-element leaky-wave antenna with constant gain and enhanced broadside radiation bandwidth using multilayered composite right/left-handed substrate integrated waveguide," *Int. J. RF Microw. Comput. Eng.*, vol. 27, no. 3, pp. 1–7, 2017.

[25] A. A. Oliner and D. R. Jackson, "Leaky-wave antennas," in *Antenna Engineering Handbook*, 4th ed., J. L. Volakis, Ed. New York, NY, USA: McGraw-Hill, 2007, ch. 11.

[26] D. R. Jackson and A. A. Oliner, "Leaky-wave antennas," in *Modern Antenna Handbook*, C. A. Balanis, Eds. Hoboken, NJ, USA: Wiley, 2008, ch. 7.

[27] M. Guglielmi and D. R. Jackson, "Broadside radiation from periodic leaky-wave antennas," *IEEE Trans. Antennas Propag.*, vol. 41, no. 1, pp. 31–37, Jan. 1993.

[28] K. Solbach and B. Adelseck, "Dielectric image line leaky wave antenna for broadside radiation," *Electron. Lett.*, vol. 19, no. 16, pp. 640–641, Aug. 1983.

[29] J. R. James and P. Hall, "Microstrip antennas and arrays, part 2: New array-design technique," *IEE J. Microw. Opt. Antennas*, vol. 1, pp. 175–181, Sep. 1977.

[30] J. R. James, P. Hall, and C. Wood, *Microstrip Antenna Theory and Design*. London, U.K.: Peregrinus, 1981.

[31] S. Paulotto, P. Baccarelli, F. Frezza, and D. R. Jackson, "A novel technique for open-stopband suppression in 1-D periodic printed leaky wave antennas," *IEEE Trans. Antennas Propag.*, vol. 57, no. 7, pp. 1894–1906, Jul. 2009.

[32] J. T. Williams, P. Baccarelli, S. Paulotto, and D. R. Jackson, "1-D combline leaky-wave antenna with the open-stopband suppressed: Design considerations and comparisons with measurements," *IEEE Trans. Antennas Propag.*, vol. 61, no. 9, pp. 4484–4492, Sep. 2013.

[33] M. H. Rahmani and D. Deslandes, "Backward to forward scanning periodic leaky-wave antenna with wide scanning range," *IEEE Trans. Antennas Propag.*, vol. 65, no. 7, pp. 3326–3335, Jul. 2017.

[34] D. K. Karmokar and K. P. Esselle, "Periodic u-slot-loaded dual-band half-width microstrip leaky-wave antennas for forward and backward beam scanning," *IEEE Trans. Antennas Propag.*, vol. 63, no. 12, pp. 5372–5381, Dec. 2015.

[35] S. Otto, A. Al-Bassam, A. Rennings, K. Solbach, and C. Caloz, "Radiation efficiency of longitudinally symmetric and asymmetric periodic leaky-wave antennas," *IEEE Antennas Wireless Propag. Lett.*, vol. 11, pp. 612–615, 2012.
[36] S. Otto, A. Al-Bassam, A. Rennings, K. Solbach, and C. Caloz, "Transversal asymmetry in periodic leaky-wave antennas for Bloch impedance and radiation efficiency equalization through broadside," *IEEE Trans. Antennas Propag.*, vol. 62, no. 10, pp. 5037–5054, Oct. 2014.
[37] S. Otto, Z. Chen, A. Al-Bassam, A. Rennings, K. Solbach, and C. Caloz, "Circular polarization of periodic leaky-wave antennas with axial asymmetry: Theoretical proof and experimental demonstration," *IEEE Trans. Antennas Propag.*, vol. 62, no. 4, pp. 1817–1829, Apr. 2014.
[38] A. Al-Bassam, S. Otto, D. Heberling, and C. Caloz, "Broadside dual-channel orthogonal-polarization radiation using a double-asymmetric periodic leaky-wave antenna," *IEEE Trans. Antennas Propag.*, vol. 65, no. 6, pp. 2855–2864, Jun. 2017.
[39] P. Baccarelli, C. Di Nallo, S. Paulotto, and D. R. Jackson, "A full-wave numerical approach for modal analysis of 1-D periodic microstrip structures," *IEEE Trans. Microw. Theory Techn.*, vol. 54, no. 4, pp. 1350–1362, Jun. 2006.
[40] N. Marcuvitz, *Waveguide Handbook*. Edison, NJ, USA: IET, 1951, pp. 285–287.
[41] M. Guglielmi and G. Boccalone, "A novel theory for dielectric-inset waveguide leaky-wave antennas," *IEEE Trans. Antennas Propag.*, vol. 39, no. 4, pp. 497–504, Apr. 1991.
[42] J. Liu, D. R. Jackson, and Y. Long, "Modal analysis of dielectric-filled rectangular waveguide with transverse slots," *IEEE Trans. Antennas Propagat.*, vol. 59, no. 9, pp. 3194–3203, Sep. 2011.
[43] D. M. Pozar, *Microwave Engineering*, 4th ed. Hoboken, NJ, USA: Wiley, 2011, ch. 8, p. 383.

Wenlong Zhou was born in Dongguan, Guangdong, China, in 1993. He received the B.S. degree in electrical engineering from Sun Yat-sen University, Guangzhou, China, in 2016, where he is currently pursuing the M.Eng. degree.

His current research interests include microstrip antennas, substrate integrated waveguide antennas, circularly polarized antennas, and leaky-wave antennas.

Juhua Liu (M'12) was born in Heyuan, Guangdong, China, in 1981. He received the B.S. and Ph.D. degrees in electrical engineering from Sun Yat-sen University, Guangzhou, China, in 2004 and 2011, respectively.

From 2008 to 2009, he was a Visiting Scholar with the Department of Electrical and Computer Engineering, University of Houston, Houston, TX, USA. From 2011 to 2012, he was a Senior Research Associate with the State Key Laboratory of Millimeter Waves, City University of Hong Kong, Hong Kong. From 2012 to 2015, he was a Lecturer with the Department of Electronics and Communication Engineering, Sun Yat-sen University, where he has been an Associate Professor since 2015. His current research interests include microstrip antennas, substrate integrated waveguide antennas, leaky-wave antennas, periodic structures, and computational electromagnetics.

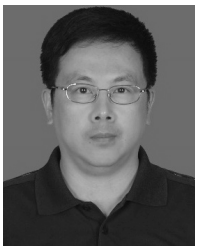

Yunliang Long (M'01–SM'02) was born in Chongqing, China, in 1963. He received the B.Sc., M.Eng., and Ph.D. degrees from the University of Electronic Science and Technology of China, Chengdu, China, in 1983, 1989, and 1992, respectively.

From 1992 to 1994, he was a Post-Doctoral Research Fellow with the Department of Electronics, Sun Yat-sen University, Guangzhou, China, where he was an Associate Professor. From 1998 to 1999, he was a Visiting Scholar with IHF, Basel, Switzerland, and with the RWTH University of Aachen, Aachen, Germany. From 2000 to 2001, he was a Research Fellow with the Department of Electronics Engineering, City University of Hong Kong, Hong Kong. He is currently a Professor and the Head of the Department of Electronics and Communication Engineering, Sun Yat-sen University. He has authored or co-authored over 130 academic papers. His current research interests include antennas and propagation theories, electromagnetic theory in inhomogeneous lossy medium, computational electromagnetics, and wireless communication applications.

Dr. Long is a member of the Committee of Microwave Society of CIE and on the Editorial Board of the *Chinese Journal of Radio Science*. He is the Vice Chairman of the Guangzhou Electronic Industrial Association. He is listed in *Who's Who in the World.*